THE JOURNAL OF PHYSICAL CHEMISTRY Letters

pubs.acs.org/JPCL

Letter

Unusual Transport Properties with Noncommutative System–Bath Coupling Operators

Chenru Duan, Chang-Yu Hsieh, Junjie Liu, Jianlan Wu, and Jianshu Cao*

Cite This: J. Phys. Chem. Lett. 2020, 11, 4080–4085

Read Online

ACCESS | Metrics & More | Article Recommendations | Supporting Information

ABSTRACT: Understanding nonequilibrium transport is crucial for controlling energy flow in nanoscale systems. We study thermal energy transfer in a generalized nonequilibrium spin-boson model (NESB) with noncommutative system–bath coupling operators and discover its unusual transport properties. Compared to the conventional NESB, the energy current is greatly enhanced by rotating the system–bath coupling operators.

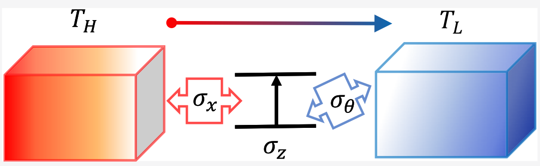

Constructive contribution to thermal rectification can be optimized when two sources of asymmetry, system–bath coupling strength and coupling operators, coexist. At the weak coupling and the adiabatic limit, the scaling dependence of energy current on the coupling strength and the system energy gap changes drastically when the coupling operators become noncommutative. These scaling relations can further be explained analytically by the nonequilibrium polaron-transformed Redfield equation (NE-PTRE). These novel transport properties, arising from the pure quantum effect of noncommutative coupling operators, suggest an unvisited dimension of controlling transport in nanoscale systems and should generally appear in other nonequilibrium set-ups and driven systems.

With the advance of nanoscale quantum technologies and global efforts on sustainable development, understanding the fundamental laws of transport at the microscopic level has attracted much theoretical and experimental attention.[1−10] Treated as a minimal model for anharmonic molecular junctions, the nonequilibrium spin-boson model (NESB) has been extensively investigated with various theoretical[11−21] and numerical methods.[22−28] Many interesting properties of energy transfer have been found, including a turnover of the energy current as the system–bath coupling strength increases.[18,25]

Symmetry is rooted in the development of physical science and plays a crucial role in both equilibrium and nonequilibrium systems.[29−33] In NESB, for example, the asymmetry of the system–bath coupling strength leads to thermal rectification.[34,35] For a spin coupled with two zero-temperature bosonic baths, nontrivial phases and quantum phase transition arise from the competition of the two asymmetric dissipation channels.[36−40] Despite the effort on studying the equilibrium state of this two-bath system with asymmetric couplings, little attention has been paid to investigate the influence of noncommutative coupling operators on transport behaviors. An exception is a recent study[24] of quantum transfer, which uses the noncommutative couplings to clarify the definition of energy current. Yet, to date, the energy-transfer properties resulting from the noncommutative coupling have not been explored.

In this Letter, we thoroughly investigate the influence of noncommutative coupling operators on transport properties in NESB using a numerically accurate method, extended hierarchy equation of motion (eHEOM).[41−44] In the weak coupling regime, a smooth linear-to-quadratic transition in the scaling relation of energy current and coupling strength is found as we rotate the system–bath coupling operators. For a generalized NESB with noncommutative coupling operators (nc-NESB), a plateau in energy current occurs when the system energy is negligibly small compared to the characteristic frequency of the bath, while the energy current drops to zero at the same condition in the conventional NESB (c-NESB). These observations can be quantitatively explained by the analytical solution of the nonequilibrium polaron-transformed Redfield equation (NE-PTRE).[18−21,45,46] The steady-state energy current of nc-NESB is significantly enhanced compared to the c-NESB by simply rotating the coupling operators between the system and bath. In addition, two sources of asymmetry, namely, asymmetric coupling strength and noncommutative coupling operators, can contribute constructively to thermal rectification, giving rise to a thermal rectification ratio larger than that in cases with only one source of asymmetry. Our results suggest a simple yet new method of controlling transport behaviors in nanoscale systems.

The Hamiltonian for a generalized NESB is

Received: March 29, 2020
Accepted: April 30, 2020
Published: April 30, 2020

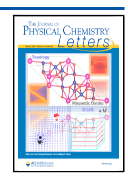

$$H = H_S + H_{B,1} + H_{B,2} + V_1 \otimes B_1 + V_2 \otimes B_2 = \Delta\sigma_z + \sum_{\nu=\{1,2\},j} \omega_{\nu,j} b_{\nu,j}^\dagger b_{\nu,j} + \sigma_x \sum_j g_{1,j}(b_{1,j}^\dagger + b_{1,j}) + \sigma_\theta \sum_j g_{2,j}(b_{2,j}^\dagger + b_{2,j}) \quad (1)$$

Here σ_i ($i = x, y, z$) denotes the Pauli matrices; Δ is the half energy gap of the two-level system, and $b_{\nu,j}^\dagger$ ($b_{\nu,j}$) is the creation (annihilation) operator of the j-th harmonic oscillator in the νth bosonic bath. We consider the effect of noncommutative coupling by introducing a parameter θ for the coupling operator between the system and the second bath, i.e., $\sigma_\theta = \sigma_z \cos\theta + \sigma_x \sin\theta$, so that it can point at any direction on the $x-z$ plane of a Bloch sphere. Because of the rotational symmetry of the model, we can restrict our study to $0 \le \theta \le \pi/2$ without loss of generality. Note that our Hamiltonian reduces to the c-NESB at $\theta = \pi/2$; otherwise, it represents an nc-NESB.

The dissipative effect on the system can be characterized by a spectral density $J_\nu(\omega) = 4\pi\sum_j g_{\nu,j}^2 \delta(\omega - \omega_{\nu,j}) = \pi\alpha_\nu \omega^s \omega_c^{1-s} f(\omega/\omega_c)$, which is defined by the dimensionless system−bath coupling strength (α_ν); the cutoff function of the environment ($f(\omega/\omega_c)$); and the spectral exponent (s) that categorizes the bath into sub-Ohmic ($s < 1$), Ohmic ($s = 1$), or super-Ohmic ($s > 1$). Throughout this Letter, we choose a super-Ohmic spectral exponent $s = 3$ and a rational cutoff function $f(\omega/\omega_c) = 1/(1 + (\omega/\omega_c)^2)^4$ for both high- and low-temperature baths and assume $\alpha_1 = \alpha_2 = \alpha$ unless specified. The atomic unit $\hbar = k_B = 1$ is used, and the bath cutoff frequency is treated as an energy unit ($\omega_c = 1$). Further, the bath correlation function, $C_\nu(t) = 1/\pi\int_0^\infty J_\nu(\omega)\left[\coth\frac{\beta_\nu\omega}{2}\cos\omega t - \mathrm{i}\sin\omega t\right]\mathrm{d}\omega$, with the inverse temperature $\beta_\nu = 1/T_\nu$, uniquely determines the bath properties and their influence on the system.

Because of its numerical accuracy in propagating the dynamics and its compatibility for energy current calculation, the HEOM has become a popular numerical method for simulating transport problems.[23,24,27,28,41] In this Letter we adopt the extended HEOM which can be applied to more general bosonic baths than the Debye−Lorentz form.[43,44,47,48] In the extended HEOM, bath correlation functions and their time derivatives are decomposed by some finite basis sets $\{\phi_{\nu,j}^X(t)\}$ where $C_\nu^X(t) = \sum_j a_{\nu,j}^X \phi_{\nu,j}^X(t)$ and $\frac{\partial}{\partial t}C_\nu^X(t) = \sum_{j,j'} a_{\nu,j}^X \eta_{\nu,j,j'}^X \phi_{\nu,j'}^X(t)$. Here, X = R or I denotes the real or imaginary part of the bath correlation function, $C_\nu(t)$. Based on those closed function sets $\{\phi_{\nu,j}^X(t)\}$, auxiliary fields, $\vec{\sigma}(t)$, can be constructed and their evolutions are expressed in a time-local form[42,49]

$$\frac{\partial}{\partial t}\vec{\sigma}(t) = \vec{\mathcal{K}}\vec{\sigma}(t) \quad (2)$$

where $\vec{\mathcal{K}}$ is a tensor that can be derived from HEOM formalism.[42,49] The energy current from a bath perspective can be further expressed with the first-order auxiliary fields[24,27,49,50]

$$I_\nu(t) = -\sum_{j,j'} a_{\nu,j}^R \eta_{\nu,j,j'}^R \sigma_1^{\vec{n}_\nu=(j')}(t) - \sum_{j,j'} a_{\nu,j}^I \eta_{\nu,j,j'}^I \sigma_1^{\vec{m}_\nu=(j')}(t) \quad (3)$$

where the steady-state energy current is obtained as $t \to +\infty$. Unlike some methods that are restricted by the system−bath coupling operators, eq 3 can be directly applied to calculate the steady-state energy current (I) for an nc-NESB. For the results presented in this work, we carefully examined our eHEOM calculations and confirmed their numerical convergence.

Figure 1a demonstrates the relationship between the steady-state energy current and the coupling strength for different nc-NESB configurations (θ). In the weak coupling regime, the energy current of c-NESB ($\theta = 0.5\pi$) is proportional to the coupling strength, $I \sim \alpha$, which agrees with the Redfield equation. Whereas for an nc-NESB, this scaling behavior is altered. At the extreme case when the two coupling operators are orthogonal ($\theta = 0$), we observe $I \sim \alpha^2$. For $0 < \theta < 0.5\pi$, there is a smooth transition from $I \sim \alpha^2$ to $I \sim \alpha$.[49] This continuous transition is implied by the energy current expression in the Heisenberg picture[24]

$$I = \langle[\Delta\sigma_z, (\sigma_z\cos\theta + \sigma_x\sin\theta) \otimes \hat{B}_2]\rangle + \langle[\sigma_x \otimes \hat{B}_1, (\sigma_z\cos\theta + \sigma_x\sin\theta) \otimes \hat{B}_2]\rangle \quad (4)$$

where $\langle\cdots\rangle$ is the trace of the steady-state total density matrix over all degrees of freedom and $\hat{B}_\nu$ denotes the bath operator in the Heisenberg picture. In the weak coupling limit, the first term in eq 4 gives linear dependence of I on α but vanishes at $\theta = 0$, where the second term predicts $I \sim \alpha_1\alpha_2 \sim \alpha^2$. As shown in Figure 1a, despite the difference in the scaling relation at small α when varying θ, the energy currents all show a turnover behavior, which can be explained by the strong damping limit of the Fermi golden rule.[51] Nevertheless, significant enhancement in the energy current can still be observed for nc-NESB ($\theta \neq 0.5\pi$) compared to that of c-NESB ($\theta = 0.5\pi$) except for a very weak coupling strength.

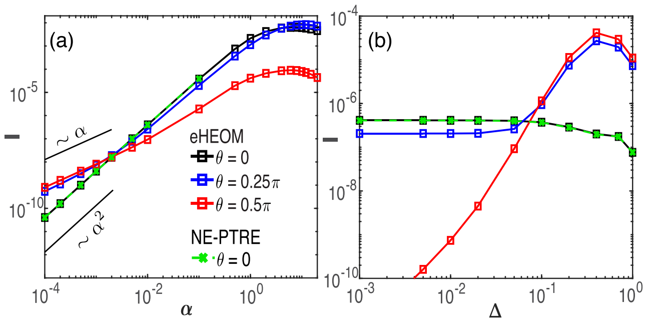

Figure 1. Energy current (I) as a function of (a) coupling strength (α) at $\Delta = 0.05$ and (b) half energy gap (Δ) at $\alpha = 0.01$ with different coupling operators for the second bath: $\theta = 0$ (black and green), $\theta = 0.25\pi$ (blue), and $\theta = 0.5\pi$ (red). Squares are results from the eHEOM, and crosses are results obtained by the NE-PTRE. Other parameters are $T_1 = 1$ and $T_2 = 0.9$. The results of eHEOM and NE-PTRE agree near perfectly at $\theta = 0$, resulting in the overlapping green and black curves. However, NE-PTRE cannot be applied to the regime of low or zero temperature.

For different NESB configurations, the Δ dependence on the energy current I is depicted in Figure 1b. For the c-NESB, I drops to zero as $\Delta \to 0$. For an nc-NESB, a plateau for the energy current appears when Δ approaches zero. This phenomena can also be explained by eq 4 in which the first term depends explicitly on Δ while the second term does not. Therefore, even though the first term becomes zero at $\Delta \to 0$, the second term, which accounts for the high-order system−

https://dx.doi.org/10.1021/acs.jpclett.0c00985
J. Phys. Chem. Lett. 2020, 11, 4080−4085

bath interaction in the presence of noncommutative coupling, can still contribute to energy transfer and lead to a nonzero energy current for nc-NESB. Physically, at $\Delta = 0$, the total Hamiltonian can simply be diagonalized for $\theta = 0.5\pi$ by a full polaron transformation, which results in a block-diagonalized matrix, thus preventing any channels for energy transfer between two baths.[52] However, this diagonalization cannot be performed when $\theta \neq 0.5\pi$, and those nondiagonal parts give rise to a nonzero energy current. Note that the Redfield equation cannot capture the second term in eq 4, which is due to high-order system−bath interaction. Therefore, it requires other methods to evaluate higher-order interaction. So we introduce the nonequilibrium polaron-transformed Redfield equation (NE-PTRE) below.[18−20]

To develop a clear physical picture of polaron transformation, we consider a specific configuration, $\theta = 0$, i. e., the two system−bath coupling operators are orthogonal, so that the first term in eq 4 vanishes. With a full polaron transformation of the second bath and the introduction of the counting field (χ) on the first bath,[53] we obtain the transformed Hamiltonian H' as[49]

$$H' = \Delta\sigma_z + \sum_{\nu,j} \omega_{\nu,j} b_{\nu,j}^\dagger b_{\nu,j} + (\sigma_x \cosh 2A_2 + i\sigma_y \sinh 2A_2) \sum_j g_{1,j}\left(b_{1,j}^\dagger\left[\frac{\chi}{2}\right] + b_{1,j}\left[\frac{\chi}{2}\right]\right) \tag{5}$$

where $A_2 = \sum_J g_{2,j}/\omega_{2,j}(b_{2,j}^\dagger - b_{2,j})$ and $O[\chi] = \exp\left(i\chi \sum_J \omega_{1,j} b_{1,j}^\dagger b_{1,j}\right) O \exp\left(-i\chi \sum_J \omega_{1,j} b_{1,j}^\dagger b_{1,j}\right)$. Following the standard procedure of the NE-PTRE[18−20] and a perturbation expansion on α, the energy current can be obtained as[49]

$$I = -2\int_0^\infty dt(C_1^R(t)\dot{Q}_2^I(t) + C_1^I(t)\dot{Q}_2^R(t))\cos 2\Delta t + 2\xi(\Delta)\int_0^\infty dt(C_1^I(t)\dot{Q}_2^I(t) + C_1^R(t)\dot{Q}_2^R(t))\sin 2\Delta t \tag{6}$$

where $\xi(\Delta) = \int_0^\infty dtC_1^I \sin 2\Delta t / \int_0^\infty dtC_1^R \cos 2\Delta t$ is independent of α and $Q_2(t) = Q_2^R(t) + iQ_2^I(t) = 2\int_0^\infty d\omega J_2(\omega)[n_2(\omega)\exp(i\omega t) + (n_2(\omega) + 1)\exp(-i\omega t)]/\omega^2$. Here we have $\dot{Q}_2^X(t) = dQ_2^X(t)/dt$ and the Bose−Einstein distribution function $n_\nu(\omega) = 1/(\exp(\beta_\nu\omega) - 1)$. On one hand, both $C_1^X(t)$ and $Q_2^X(t)$ are linearly dependent on the coupling strength α, giving $I \sim \alpha^2$ in Figure 1a. On the other hand, eq 6 clearly predicts a nonvanishing energy current $I(\Delta = 0) = -2\int_0^\infty dt(C_1^R(t)\dot{Q}_2^I(t) + C_1^I(t)\dot{Q}_2^R(t)$. In the adiabatic limit of $\Delta \ll 1$, we have $I(\Delta \ll 1) - I(\Delta = 0) \sim \Delta^2$, which explains the plateau in Figure 1b. As shown in Figure 1, results obtained by eq 6 are in excellent agreement with those of the extended HEOM. The domain of application with only $\Delta \ll 1$ was previously an issue in NE-PTRE but recently was resolved in the variational version.[21] As a result, our energy current expression (eq 6) is not limited to small $\Delta \ll 1$ as it does not involve perturbative expansion of Δ. However, because only the second bath is displaced in polaron transformation, NE-PTRE cannot be applied to the low- or zero-temperature regime.

Optimal thermal properties are always of great interest to the performance of molecular junctions, quantum heat engines, and heat pumps.[7] In our model, energy current can be optimized with respect to θ, given that other parameters (α, Δ, T_1, and T_2) are fixed. Figure 2 demonstrates various behaviors

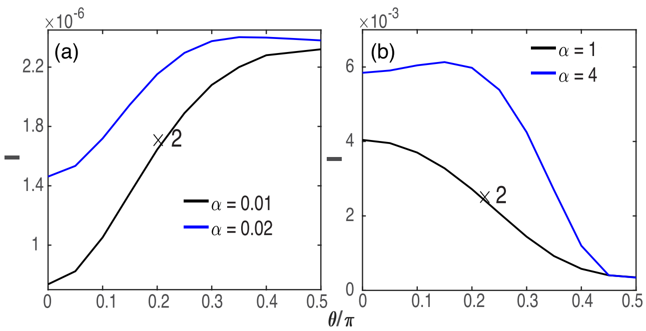

Figure 2. Energy current as a function of the second operator direction θ: (a) $\alpha = 0.01$ (black) and $\alpha = 0.02$ (blue); (b) $\alpha = 1$ (black) and $\alpha = 4$ (blue). Black lines in both panels a and b are multiplied by a factor of 2 for a better view of the results. Other parameters are $T_1 = 1$, $T_2 = 0.9$, and $\Delta = 0.1$.

of energy current as we rotate the second coupling operator from σ_z to σ_x direction at a fixed energy gap $\Delta = 0.1$. At a very weak coupling strength of $\alpha = 0.01$, the energy current grows monotonously as θ increases from 0 to 0.5π.[24] In contrast, for $\alpha = 1$, the energy current decreases monotonically with increasing θ. Nonmonotonous θ dependence emerges for $\alpha = 0.02$ and $\alpha = 4$, where the energy current is maximal at an intermediate configuration, i.e., $0 < \theta_{opt} < \pi/2$.

To develop a better understanding of the optimal energy-transfer behavior, we further study the relationship between the coupling strength and the optimal angle, θ_{opt}, at which the energy current reaches its maximum value I_{opt}. Results are shown in Figure 3a. For a finite Δ, four distinct regimes can be

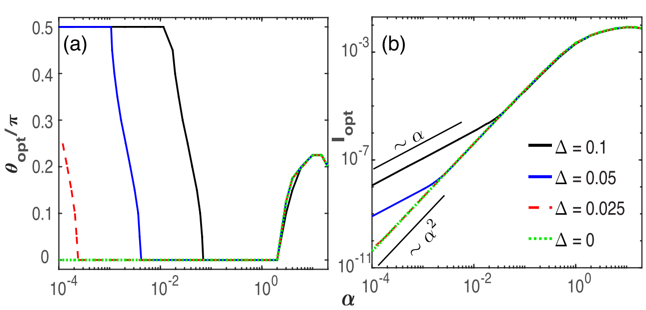

Figure 3. Coupling strength dependence of the (a) optimized angle and (b) optimized energy current for a series of Δ at the scaling limit: $\Delta = 0.1$ (black solid line), $\Delta = 0.05$ (blue solid line), $\Delta = 0.025$ (red dashed line), and $\Delta = 0$ (green dotted line). Temperatures for the two baths are $T_1 = 1$ and $T_2 = 0.9$, respectively.

identified over the range of the coupling strength under investigation, which reflect the interplay of the two terms in the energy current expression (eq 4) for nc-NESB. (I) For a very weak system−bath coupling, the c-NESB ($\theta = 0.5\pi$) gives the maximal energy current, because the linear term in eq 4 is dominant in comparison with the second-order term. (II) A transition of the optimal angle from $\theta_{opt} = 0.5\pi$ to $\theta_{opt} = 0$ follows with the increasing coupling strength, because of the non-negligible contribution from the second-order term in eq

https://dx.doi.org/10.1021/acs.jpclett.0c00985
J. Phys. Chem. Lett. 2020, 11, 4080−4085

4. (III) The effect of second-order energy current is prominent within a certain range of α where the optimal angle stays at $\theta_{opt} = 0$. (IV) The contributions of even higher-order transport processes gradually intervene and eventually become dominant at very strong coupling strength, so that $0 < \theta_{opt} < 0.5\pi$ can be observed. These four regimes are also indicated in Figure 3b, which depicts the relationship between α and I_{opt}: $I_{opt} \sim \alpha$ at the very weak interaction (I) followed by a transition (II) to $I_{opt} \sim \alpha^2$ (III) at the intermediate coupling strength. As the system−bath interaction keeps increasing, I_{opt} deviates from the α^2 dependence and a turnover appears (IV). Although this turnover behavior is inevitable because of the inseparability between system and bath, the maximum energy current, $I_{max} = \max\{I_{opt}(\alpha)\}$, can be greatly enhanced when considering an nc-NESB (see Figure 1a). It is also interesting to note that I_{opt} and θ_{opt} is insensitive to the value of Δ except for very weak coupling strength (I), which is in sharp contrast to the case of c-NESB.[12] This indicates a rather robust global energy current optimization I_{max} for $\{\alpha, \Delta, \theta\}$ once the bath temperatures are given, which might find practical utility in molecular junction engineering.

As Δ decreases, the transition between regime I and regime II occurs earlier and is sharper (Figure 3b). This transition finally disappears, and there are only regime III and regime IV left for a system with zero energy gap, which can be explained by eq 4. At $\Delta = 0$, the contribution of the first term vanishes and only the second term survives, which is most pronounced when the two coupling operators commute with each other, i.e., $\theta = 0$. It can be expected that more diverse energy current behaviors will occur if we do not constrain the second bath operator lying in the x−z plane of the Bloch sphere and allow the rotation of both coupling operators.

Thermal rectification, which arises from the asymmetry in the total Hamiltonian, offers rich possibilities to manipulate energy flow in nanoscale systems.[34,35,54] The extent of thermal rectification can be measured by the rectification ratio, which is the ratio of the two steady-state energy currents before and after the temperatures of two baths are exchanged. In the c-NESB, the thermal rectification is usually realized by the asymmetry in coupling strength.[13,34] Here we introduce a novel source of asymmetry, noncommutative coupling operators between the system and two baths. Figure 4 demonstrates the thermal rectification ratio for the c-NESB ($\theta = 0.5\pi$) and an nc-NESB with $\theta = 0.125\pi$. A nonvanishing rectification occurs for the nc-NESB even at $\alpha_1 = \alpha_2$, which is a

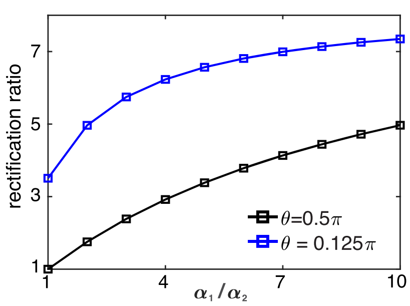

Figure 4. Thermal rectification for NESB with two different coupling operators: $\theta = 0.5\pi$ (black) and $\theta = 0.125\pi$ (blue). Rectification ratio is defined as the ratio between two values of energy current with the exchange of bath temperatures T_1 and T_2. We fix $\alpha_1 = 0.01$ and vary α_2 to obtain different ratios of α_1/α_2. Other parameters are $T_1 = 10$, $T_2 = 1$, and $\Delta = 0.5$.

pure quantum effect due to the asymmetry in coupling operators. More interestingly, the rectification ratio at $\theta = 0.125\pi$ is significantly larger than that of the c-NESB for the entire parameter space. This implies that two sources of asymmetry, coupling strength and coupling operators, can work constructively to achieve optimal rectification.

In conclusion, we study transport properties of a generalized NESB with noncommutative system−bath coupling operators and find unique behaviors that are different from those of the conventional NESB. Scaling behaviors of the energy current with respect to the coupling strength and the system energy gap are significantly altered when the two coupling operators do not commute, giving $I \sim \alpha^2$ in the weak coupling limit and $I(\Delta \to 0^+) \neq 0$ in the adiabatic limit, in sharp contrast to $I \sim \alpha$ and $I(\Delta \to 0^+) \to 0$ for the conventional NESB. These scaling relations can be explained analytically by the NE-PTRE. Optimization for the energy current is performed using the extended HEOM, and four different regimes are distinguished. Given the temperatures of two baths, a robust global optimal energy current can be obtained, independent of the system energy gap. The energy current can be significantly enhanced with proper manipulation of the system−bath coupling operators. The effect of asymmetry originating from both the asymmetrical coupling strength and noncommutative coupling operators can contribute constructively to thermal rectification, resulting in an enhanced rectification ratio. The enhancement of energy current and thermal rectification due to the noncommutative coupling offers new and potentially advanced techniques for energy flow control. We emphasize that these unusual transport properties reported in this work are caused solely by the quantum effect of commutation and can also be found in other nanoscale systems, including quantum heat engines and periodically driven systems.[51,55] While the focus of this work is the novel steady-state transport behaviors, the noncommutative system−bath coupling also affects the dynamic behavior in nonequilibrium transport, which will be explored in future work.

■ ASSOCIATED CONTENT

Supporting Information

The Supporting Information is available free of charge at https://pubs.acs.org/doi/10.1021/acs.jpclett.0c00985.

Derivation of energy current expression by the extended hierarchy equation of motion; derivation of energy current expression by the nonequilibrium polaron-transformed Redfield equation; demonstration of the smooth transition for the energy current linear-to-quadratic scaling dependence on the coupling strength (PDF)

■ AUTHOR INFORMATION

Corresponding Author

Jianshu Cao − *Department of Chemistry, Massachusetts Institute of Technology, Cambridge, Massachusetts 02139, United States; Singapore-MIT Alliance for Research and Technology (SMART) Center, Singapore 138602;* orcid.org/0000-0001-7616-7809; Email: jianshu@mit.edu

Authors

Chenru Duan − *Department of Chemistry, Massachusetts Institute of Technology, Cambridge, Massachusetts 02139, United States; Singapore-MIT Alliance for Research and*

https://dx.doi.org/10.1021/acs.jpclett.0c00985
J. Phys. Chem. Lett. 2020, 11, 4080−4085

Technology (SMART) Center, Singapore 138602; Physics Department, Zhejiang University, Hangzhou, Zhejiang 310027, China; orcid.org/0000-0003-2592-4237

Chang-Yu Hsieh − *Singapore-MIT Alliance for Research and Technology (SMART) Center, Singapore 138602*

Junjie Liu − *Singapore-MIT Alliance for Research and Technology (SMART) Center, Singapore 138602*

Jianlan Wu − *Physics Department, Zhejiang University, Hangzhou, Zhejiang 310027, China*

Complete contact information is available at: https://pubs.acs.org/10.1021/acs.jpclett.0c00985

Notes

The authors declare no competing financial interest.

■ ACKNOWLEDGMENTS

C.D., J.L., and C.-Y.H. acknowledge support from the Singapore-MIT Alliance for Research and Technology (SMART). J.C. is supported by NSF (Grant No. CHE 1800301 and CHE 1836913) and SMART.

■ REFERENCES

(1) Ono, K.; Austing, D. G.; Tokura, Y.; Tarucha, S. Current Rectification by Pauli Exclusion in a Weakly Coupled Double Quantum Dot System. *Science* **2002**, *297*, 1313−1317.

(2) Büttner, F.; Lemesh, I.; Schneider, M.; Pfau, B.; Günther, C. M.; Hessing, P.; Geilhufe, J.; Caretta, L.; Engel, D.; Krüger, B.; et al. Field-Free Deterministic Ultrafast Creation of Magnetic Skyrmions by Spin-Orbit Torques. *Nat. Nanotechnol.* **2017**, *12*, 1040−1044.

(3) Guardado-Sanchez, E.; Morningstar, A.; Spar, B. M.; Brown, P. T.; Huse, D. A.; Bakr, W. S. Subdiffusion and Heat Transport in a Tilted Two-Dimensional Fermi-Hubbard System. *Phys. Rev. X* **2020**, *10*, 011042.

(4) Fong, K. Y.; Li, H.-K.; Zhao, R.; Yang, S.; Wang, Y.; Zhang, X. Phonon Heat Transfer across a Vacuum through Quantum Fluctuations. *Nature* **2019**, *576*, 243−247.

(5) Ronzani, A.; Karimi, B.; Senior, J.; Chang, Y.-C.; Peltonen, J. T.; Chen, C.; Pekola, J. P. Tunable Photonic Heat Transport in a Quantum Heat Valve. *Nat. Phys.* **2018**, *14*, 991−995.

(6) Bermudez, A.; Bruderer, M.; Plenio, M. B. Controlling and Measuring Quantum Transport of Heat in Trapped-Ion Crystals. *Phys. Rev. Lett.* **2013**, *111*, 040601.

(7) Dubi, Y.; Di Ventra, M. Colloquium: Heat Flow and Thermoelectricity in Atomic and Molecular Junctions. *Rev. Mod. Phys.* **2011**, *83*, 131−155.

(8) Roßnagel, J.; Dawkins, S. T.; Tolazzi, K. N.; Abah, O.; Lutz, E.; Schmidt-Kaler, F.; Singer, K. A Single-Atom Heat Engine. *Science* **2016**, *352*, 325−329.

(9) Pandey, H. D.; Leitner, D. M. Thermalization and Thermal Transport in Molecules. *J. Phys. Chem. Lett.* **2016**, *7*, 5062−5067.

(10) Talkner, P.; Hanggi, P. Colloquium: Statistical Mechanics and Thermodynamics at Strong Coupling: Quantum and Classical. *arXiv*, **2019**, 1911.11660. http://arxiv.org/abs/1911.11660 (accessed 2020-04-21).

(11) Nicolin, L.; Segal, D. Quantum Fluctuation Theorem for Heat Exchange in the Strong Coupling Regime. *Phys. Rev. B: Condens. Matter Mater. Phys.* **2011**, *84*, 161414.

(12) Boudjada, N.; Segal, D. From Dissipative Dynamics to Studies of Heat Transfer at the Nanoscale: Analysis of the Spin-Boson Model. *J. Phys. Chem. A* **2014**, *118*, 11323−11336.

(13) Agarwalla, B. K.; Segal, D. Energy Current and its Statistics in the Nonequilibrium Spin-Boson Model: Majorana Fermion Representation. *New J. Phys.* **2017**, *19*, 043030.

(14) Ruokola, T.; Ojanen, T. Thermal Conductance in a Spin-Boson Model: Cotunneling and Low-Temperature Properties. *Phys. Rev. B: Condens. Matter Mater. Phys.* **2011**, *83*, 045417.

(15) Thingna, J.; Zhou, H.; Wang, J.-S. Improved Dyson Series Expansion for Steady-State Quantum Transport beyond the Weak Coupling Limit: Divergences and Resolution. *J. Chem. Phys.* **2014**, *141*, 194101.

(16) Liu, J.; Xu, H.; Li, B.; Wu, C. Energy Transfer in the Nonequilibrium Spin-Boson Model: From Weak to Strong Coupling. *Phys. Rev. E: Stat. Phys., Plasmas, Fluids, Relat. Interdiscip. Top.* **2017**, *96*, 012135.

(17) Esposito, M.; Ochoa, M. A.; Galperin, M. Quantum Thermodynamics: A Nonequilibrium Green's Function Approach. *Phys. Rev. Lett.* **2015**, *114*, 080602.

(18) Wang, C.; Ren, J.; Cao, J. Nonequilibrium Energy Transfer at Nanoscale: A Unified Theory from Weak to Strong Coupling. *Sci. Rep.* **2015**, *5*, 11787.

(19) Xu, D.; Wang, C.; Zhao, Y.; Cao, J. Polaron Effects on the Performance of Light-Harvesting Systems: A Quantum Heat Engine Perspective. *New J. Phys.* **2016**, *18*, 023003.

(20) Wang, C.; Ren, J.; Cao, J. Unifying Quantum Heat Transfer in a Nonequilibrium Spin-Boson Model with Full Counting Statistics. *Phys. Rev. A: At., Mol., Opt. Phys.* **2017**, *95*, 023610.

(21) Hsieh, C.-Y.; Liu, J.; Duan, C.; Cao, J. A Nonequilibrium Variational Polaron Theory to Study Quantum Heat Transport. *J. Phys. Chem. C* **2019**, *123*, 17196−17204.

(22) Saito, K.; Kato, T. Kondo Signature in Heat Transfer via a Local Two-State System. *Phys. Rev. Lett.* **2013**, *111*, 214301.

(23) Kato, A.; Tanimura, Y. Quantum Heat Transport of a Two-Qubit System: Interplay between System-Bath Coherence and Qubit-Qubit Coherence. *J. Chem. Phys.* **2015**, *143*, 064107.

(24) Kato, A.; Tanimura, Y. Quantum Heat Current under Non-Perturbative and Non-Markovian Conditions: Applications to Heat Machines. *J. Chem. Phys.* **2016**, *145*, 224105.

(25) Velizhanin, K. A.; Wang, H.; Thoss, M. Heat Transport through Model Molecular Junctions: A Multilayer Multiconfiguration Time-Dependent Hartree Approach. *Chem. Phys. Lett.* **2008**, *460*, 325−330.

(26) Xu, D.; Cao, J. Non-Canonical Distribution and Non-Equilibrium Transport beyond Weak System-Bath Coupling Regime: A Polaron Transformation Approach. *Front. Phys.* **2016**, *11*, 110308.

(27) Cerrillo, J.; Buser, M.; Brandes, T. Nonequilibrium Quantum Transport Coefficients and Transient Dynamics of Full Counting Statistics in the Strong-Coupling and Non-Markovian Regimes. *Phys. Rev. B: Condens. Matter Mater. Phys.* **2016**, *94*, 214308.

(28) Song, L.; Shi, Q. Hierarchical Equations of Motion Method Applied to Nonequilibrium Heat Transport in Model Molecular Junctions: Transient Heat Current and High-Order Moments of the Current Operator. *Phys. Rev. B: Condens. Matter Mater. Phys.* **2017**, *95*, 064308.

(29) Gross, D. J. The Role of Symmetry in Fundamental Physics. *Proc. Natl. Acad. Sci. U. S. A.* **1996**, *93*, 14256−14259.

(30) Denisov, S.; Flach, S.; Hanggi, P. Tunable Transport with Broken Space−Time Symmetries. *Phys. Rep.* **2014**, *538*, 77−120.

(31) Walschaers, M.; Diaz, J. F.-d.-C.; Mulet, R.; Buchleitner, A. Optimally Designed Quantum Transport across Disordered Networks. *Phys. Rev. Lett.* **2013**, *111*, 180601.

(32) Thingna, J.; Manzano, D.; Cao, J. Dynamical Signatures of Molecular Symmetries in Nonequilibrium Quantum Transport. *Sci. Rep.* **2016**, *6*, 28027.

(33) Lehmann, J.; Kohler, S.; Hänggi, P.; Nitzan, A. Molecular Wires Acting as Coherent Quantum Ratchets. *Phys. Rev. Lett.* **2002**, *88*, 228305.

(34) Segal, D.; Nitzan, A. Spin-Boson Thermal Rectifier. *Phys. Rev. Lett.* **2005**, *94*, 034301.

(35) Li, N.; Ren, J.; Wang, L.; Zhang, G.; Hänggi, P.; Li, B. Colloquium: Phononics: Manipulating Heat Flow with Electronic Analogs and beyond. *Rev. Mod. Phys.* **2012**, *84*, 1045−1066.

(36) Kohler, H.; Hackl, A.; Kehrein, S. Nonequilibrium Dynamics of a System with Quantum Frustration. *Phys. Rev. B: Condens. Matter Mater. Phys.* **2013**, *88*, 205122.

(37) Guo, C.; Weichselbaum, A.; von Delft, J.; Vojta, M. Critical and Strong-Coupling Phases in One- and Two-Bath Spin-Boson Models. *Phys. Rev. Lett.* **2012**, *108*, 160401.
(38) Bruognolo, B.; Weichselbaum, A.; Guo, C.; von Delft, J.; Schneider, I.; Vojta, M. Two-Bath Spin-Boson Model: Phase Diagram and Critical Properties. *Phys. Rev. B: Condens. Matter Mater. Phys.* **2014**, *90*, 245130.
(39) Novais, E.; Castro Neto, A. H.; Borda, L.; Affleck, I.; Zarand, G. Frustration of Decoherence in Open Quantum Systems. *Phys. Rev. B: Condens. Matter Mater. Phys.* **2005**, *72*, 014417.
(40) Castro Neto, A. H.; Novais, E.; Borda, L.; Zaránd, G.; Affleck, I. Quantum Magnetic Impurities in Magnetically Ordered Systems. *Phys. Rev. Lett.* **2003**, *91*, 096401.
(41) Tanimura, Y.; Kubo, R. Time Evolution of a Quantum System in Contact with a Nearly Gaussian-Markoffian Noise Bath. *J. Phys. Soc. Jpn.* **1989**, *58*, 101−114.
(42) Tanimura, Y. Stochastic Liouville, Langevin, Fokker−Planck, and Master Equation Approaches to Quantum Dissipative Systems. *J. Phys. Soc. Jpn.* **2006**, *75*, 082001.
(43) Tang, Z.; Ouyang, X.; Gong, Z.; Wang, H.; Wu, J. Extended Hierarchy Qquation of Motion for the Spin-Boson Model. *J. Chem. Phys.* **2015**, *143*, 224112.
(44) Duan, C.; Tang, Z.; Cao, J.; Wu, J. Zero-Temperature Localization in a Sub-Ohmic Spin-Boson Model Investigated by an Extended Hierarchy Equation of Motion. *Phys. Rev. B: Condens. Matter Mater. Phys.* **2017**, *95*, 214308.
(45) Engelhardt, G.; Cao, J. Tuning the Aharonov-Bohm Effect with Dephasing in Nonequilibrium Transport. *Phys. Rev. B: Condens. Matter Mater. Phys.* **2019**, *99*, 075436.
(46) Thingna, J.; Manzano, D.; Cao, J. Magnetic Field Induced Symmetry Breaking in Nonequilibrium Quantum Networks. *arXiv*, **2019**, 1909.09549. http://arxiv.org/abs/1909.09549 (accessed 2020-04-26).
(47) Duan, C.; Wang, Q.; Tang, Z.; Wu, J. The Study of an Extended Hierarchy Equation of Motion in the Spin-Boson Model: The Cutoff Function of the Sub-Ohmic Spectral Density. *J. Chem. Phys.* **2017**, *147*, 164112.
(48) Hsieh, C.-Y.; Cao, J. A Unified Stochastic Formulation of Dissipative Quantum Dynamics. I. Generalized Hierarchical Equations. *J. Chem. Phys.* **2018**, *148*, 014103.
(49) See the Supporting Information for details of the extended HEOM and the NE-PTRE. The α dependence on I is also demonstrated with different $0 < \theta < 0.5\pi$.
(50) Kato, A.; Tanimura, Y. In *Thermodynamics in the Quantum Regime: Fundamental Aspects and New Directions*; Binder, F., Correa, L. A., Gogolin, C., Anders, J., Adesso, G., Eds.; Springer International Publishing: Cham, 2018; pp 579−595.
(51) Gelbwaser-Klimovsky, D.; Aspuru-Guzik, A. Strongly Coupled Quantum Heat Machines. *J. Phys. Chem. Lett.* **2015**, *6*, 3477−3482.
(52) Anderson, P. W. Infrared Catastrophe in Fermi Gases with Local Scattering Potentials. *Phys. Rev. Lett.* **1967**, *18*, 1049−1051.
(53) Esposito, M.; Harbola, U.; Mukamel, S. Nonequilibrium Fluctuations, Fluctuation Theorems, and Counting Statistics in Quantum Systems. *Rev. Mod. Phys.* **2009**, *81*, 1665−1702.
(54) He, D.; Thingna, J.; Cao, J. Interfacial Thermal Transport with Strong System-Bath Coupling: A Phonon Delocalization Effect. *Phys. Rev. B: Condens. Matter Mater. Phys.* **2018**, *97*, 195437.
(55) Engelhardt, G.; Platero, G.; Cao, J. Discontinuities in Driven Spin-Boson Systems due to Coherent Destruction of Tunneling: Breakdown of the Floquet-Gibbs Distribution. *Phys. Rev. Lett.* **2019**, *123*, 120602.

https://dx.doi.org/10.1021/acs.jpclett.0c00985
J. Phys. Chem. Lett. 2020, 11, 4080−4085